IEEE Photonics Journal
An IEEE Photonics Society Publication

Open Access

Fano Resonance Based on Long Range Surface Phonon Resonance in the Mid-Infrared Region

Volume 11, Number 2, April 2019

Xiangli Zhang
Yuhan Wang
Xiang Zhao
Tianye Huang
Shuwen Zeng
Perry Shum Ping

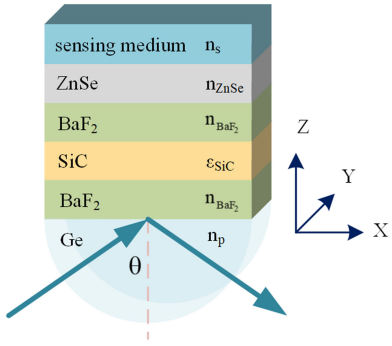

DOI: 10.1109/JPHOT.2019.2907325
1943-0655 © 2019 IEEE

IEEE photonics SOCIETY

IEEE

Fano Resonance Based on Long Range Surface Phonon Resonance in the Mid-Infrared Region

Xiangli Zhang,[1] Yuhan Wang,[1] Xiang Zhao,[1] Tianye Huang ,[1,2] Shuwen Zeng ,[3] and Perry Shum Ping[4]

[1]School of Mechanical Engineering and Electronic Information, China University of Geosciences, Wuhan 430074, China
[2]Hubei Key Laboratory of Inland Shipping Technology, Wuhan 430063, China
[3]XLIM Research Institute, University of Limoges, Limoges 87032, France
[4]Center of Fiber Technology, School of Electrical and Electronic Engineering, Nanyang Technological University, Singapore 639798

DOI:10.1109/JPHOT.2019.2907325

Manuscript received February 1, 2019; revised March 14, 2019; accepted March 21, 2019. Date of publication April 1, 2019; date of current version April 11, 2019. This work was supported in part by the Wuhan Science and Technology Bureau under Grant 2018010401011297; in part by the National Natural Science Foundation of China under Grant 61605179; in part by the Found of Hubei Key Laboratory of Inland Shipping Technology under Grant NHHY2008002; in part by the Fundamental Research Funds for the Central Universities, China University of Geosciences (Wuhan) under Grants 162301132703, G1323511794, and CUG2018JM16; and in part by the Experimental Technology Research Funds under Grant SJ-201816. Corresponding author: T. Huang (e-mail: tianye_huang@163.com.)

Abstract: Surface plasmon polaritons with noble metals lack the capability to restrain an optical field in the long wavelength region, while surface phonon polaritons with polar dielectric crystals have been regarded as a potential low-loss alternative. In this paper, long range surface phonon resonance (LRSPhR) is designed to operate in the mid-infrared (MIR) wavelength regime with a narrow resonance dip. Furthermore, by coupling a photonic waveguide with the LRSPhR, strong coupling between waveguide mode and long-range surface phonon polariton has been realized to form high Q Fano resonance. By employing such structure as the index sensor, it is shown that the bulk sensitivity and surface sensitivity can reach ~9000 and 266.9 RIU^{-1}, respectively, which shows a great enhancement comparing with the one based on merely LRSPhR. The proposed configuration can be a promising platform for MIR biochemical sensing.

Index Terms: Fano resonance, mid-infrared, waveguide mode, long-range surface phonon resonance.

1. Introduction

Surface plasmons (SP) are coherent delocalized electron oscillations excited by incident light, and charge density exists along the metal-dielectric interface with an exponentially decaying electric field [1]–[3]. In the recent years, sensors operating in the mid-infrared (MIR) regime have received particular research interests because many applications, in the fields of medicine, environmental monitoring, and security are required to work in this regime [4]–[9]. Although the noble metals, like gold and silver, can provide well-confined evanescent field at visible and near-infrared wavelength regime so as to excite the surface plasmon resonance (SPR), they perform closely to the perfect conductors and suffers from large intrinsic losses in longer wavelength, e.g., MIR, resulting in

difficulty to support surface waves [10], [11]. In order to implement sensors in MIR, polar dielectric crystals, which can be used to support surface phonon polariton (SPhP) are identified as potential low-loss alternatives [12], [13]. In polar dielectric crystals, a high reflectivity and negative real part of permittivity can be observed at specific wavelength, and the SPhP mode results from the coupling between the electromagnetic (EM) fields and optical phonons of the polar crystal [14]. Similar with SPR, conventional surface phonon resonance (SPhR) demonstrates a resonance spectrum with Lorentz shape. For sensing application, a sharp resonance is preferred to enhance the sensing accuracy. For this purpose, various methods have been proposed in the past few years, including long-range surface plasmon resonance (LRSPR) [15], [16], gold-silver bimetallic hybrid structures [17], [18], transition metal dichalcogenides (TMDCs) structures [19], [20] and so on. Besides these approaches, in recent years, Fano resonance (FR) is proved to be a promising one to further enhance the sensing performance by significantly narrowing resonance [21]–[24]. Typically, FR originates from the coupling between a dark mode and a bright mode and features an asymmetrical lineshape with a drastic slope near the resonance. In multilayer structures, FR is usually formed by the coupling between SPR/SPhR and waveguide mode resonance (WGMR), which acts as bright mode and dark mode, respectively. For example, Huang *et al.* proposed a waveguide-coupled SPR configuration, resulting in electromagnetically induced transparence and asymmetric FR. In this configuration, phase sensitivity up to 10^6 deg/RIU order with a minimum SPR reflectivity higher than 20% is achieved [25]. Hayashi *et al.* designed a multilayer structure, allowing coupling between SPP and waveguide mode (WGM). The maximum sensitivity can reach 1.5×10^3 RIU^{-1}, two orders of magnitude relative to that of conventional SPR sensors [26]. Nesterenko et al. presented a planar sensing structure in Kretschmann configuration and performs numerical and analytical study of the losses imposed to the waveguide. The maximum of the estimated sensitivity by intensity is found to be five orders of magnitude higher compared with SPR and waveguide-coupled SPR sensors [27]. Hayashi *et al.* reported on the experimental observation of the Fano line shapes in planar multilayer systems, which is shown to depend strongly on the structural parameters, and matches well with the electromagnetic calculations [28]. Wu *et al.* proposed an ultrasensitive biosensor based on hybrid structure, which is composed of long-range surface plasmon polariton (LRSPP) and dielectric planar waveguide (PWG) modes [29]. Sekkat *et al.* designed a multilayer structure formed by a metal film and a high-index dielectric waveguide, which offers the narrow Fano line shapes and a giant field intensity enhancement at the surface [30].

In this paper, we show that by using symmetric geometry, a kind of surface phonon resonance known as long-range surface phonon resonance (LRSPhR) can be excited in MIR. Similar with LR-SPR, the LRSPhR possesses much lower loss than the conventional SPhR and therefore demonstrating a resonance with narrow full width at half maximum (FWHM). By using this phenomenon, a hybrid waveguide-coupled long-range SPhR (WG-LRSPhR) sensor based on Kretschmann configuration in MIR is proposed. The coupling between WGM and LRSPhP leads to FR and its characteristics can be engineered by the multilayered structure. With extremely narrowed linewidth, the proposed system shows excellent sensing performance with intensity sensitivity up to $\sim$9000 RIU^{-1}, corresponding to five orders enhancement comparing with the one merely based on LR-SPhR.

2. Principle

The schematics of the WG-LRSPhR structure is shown in Fig. 1(a), which is a typical Kretschmann geometry. The structure consists of a germanium (Ge) prism, barium fluoride (BaF_2), silicon carbide (SiC) layer, barium fluoride (BaF_2), zinc selenide (ZnSe), and the sensing medium layer. The physical parameters are the thickness of BaF_2 layer ($d_1 = 4$ μm), SiC layer ($t = 0.7$ μm), BaF_2 layer (d_2), ZnSe layer (d_3). The SiC layer is sandwiched between two BaF_2 layers to form asymmetric structure so as to support LRSPhP modes propagating along the dielectric-SiC-dielectric interface, which is similar to a conventional LRSPhR sensor. ZnSe layer is surrounded by BaF_2 and sensing medium layer. The refractive index of ZnSe is larger than BaF_2 and sensing medium, therefore, it

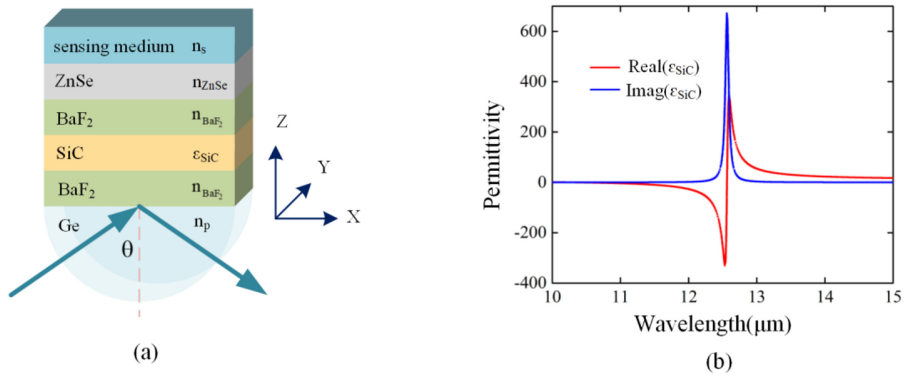

Fig. 1. (a) Structure of the multilayer sensor consisting of the Ge prism, BaF_2, SiC, BaF_2, ZnSe, sensing medium. (b) The real and imaginary parts of the permittivity of SiC, following the Drude-Lorentz model.

can support the WGM. By properly choosing the optical constants of the materials and the layer thickness, LRSPhP and WGM can be well coupled to form hybrid structure.

In the absence of free charge carriers, SiC has a frequency dependent complex permittivity which can be expressed by the Drude-Lorentz model [31]

$$\varepsilon_{\text{Sic}} = \varepsilon'_{\text{Sic}} + i\varepsilon''_{\text{Sic}} = \varepsilon_\infty \frac{\omega^2 - \omega_{\text{LO}}^2 + i\gamma\omega}{\omega^2 - \omega_{\text{ro}}^2 + i\gamma\omega} \tag{1}$$

where the longitudinal optical phonon frequency $\omega_{\text{LO}} = 972\ \text{cm}^{-1}$, the transverse optical phonon frequency is $\omega_{\text{TO}} = 796\ \text{cm}^{-1}$, the damping rate due to vibrational and harmonicity is $\gamma = 3.75\ \text{cm}^{-1}$, and the high-frequency dielectric constant $\varepsilon_\infty = 6.5$. The Reststrahlen band defined by $\varepsilon'_{\text{SiC}} < 0$ corresponding to $\omega_{\text{TO}} < \omega < \omega_{\text{LO}}$ is shown in Fig. 1(b). With $\lambda = 10.8\ \mu$m, the dispersion formulas of the refractive indexes used are $n_{\text{p}} = 4.0037$ for the Ge prism, $n_{\text{BaF2}} = 1.3919$ for the BaF_2 film, $n_{\text{ZnSe}} = 2.3950$ for the ZnSe layer [22], [32], and $n_{\text{s}} = 1.332$ for the sensing medium. Fig. 1(b) represents the real and imaginary parts of the permittivity of SiC.

3. Results and Discussions

With the absence of ZnSe layer, the structure represents a typical LRSPhR configuration. For the attenuated total reflection (ATR) curve calculation, the transfer matrix method is employed [19], [33]. With a BaF_2 thickness $d_2 = 12\ \mu$m and wavelength of 10.8 μm, the ATR curve under TM-polarized incident light is shown in Fig. 2(a) and (b). The minimum reflectivity appears at the angle of 23.1958°, illustrating the excitation of LRSPhP mode at the BaF_2-SiC-BaF_2 interface. In this condition there is no WGM because of the absence of ZnSe layer. However, the situation changes when ZnSe layer is present. According to the ATR curve of the WG-LRSPhR configuration shown in Fig. 2(b), with the thickness of ZnSe $d_3 = 1.7\ \mu$m, a sharp asymmetric FR appears at the left side of the LRSPhR. To further study the performance of the WG-LRSPhR, the amplitude distributions of the $|H_y|$ field corresponding to three resonant angles denoted as “A”, “B”, “C” are illuminated in Fig. 2(c) and (e), respectively, where the value of Z-axis represents the distance from each layer to the prism surface. There are strong electric fields concentrated in a certain region, with prominent differences in terms of the distribution profiles. Specifically, point “A” and “B” correspond to the angles of 22.8719° and 22.8762°, respectively. The fields are mainly distributed near SiC and ZnSe layers, forming LRSPhR-WGM hybrid modes, as shown in Fig. 2(c) and (d). Therefore, the coupling between the LRSPhP and WG mode is expected to take place. However, at point “C”, Fig. 2(e) demonstrates that the strong electric field is only generated at the BaF_2-SiC-BaF_2 interface and decays exponentially away from the interface, which clearly indicates the excitation of LRSPhP mode.

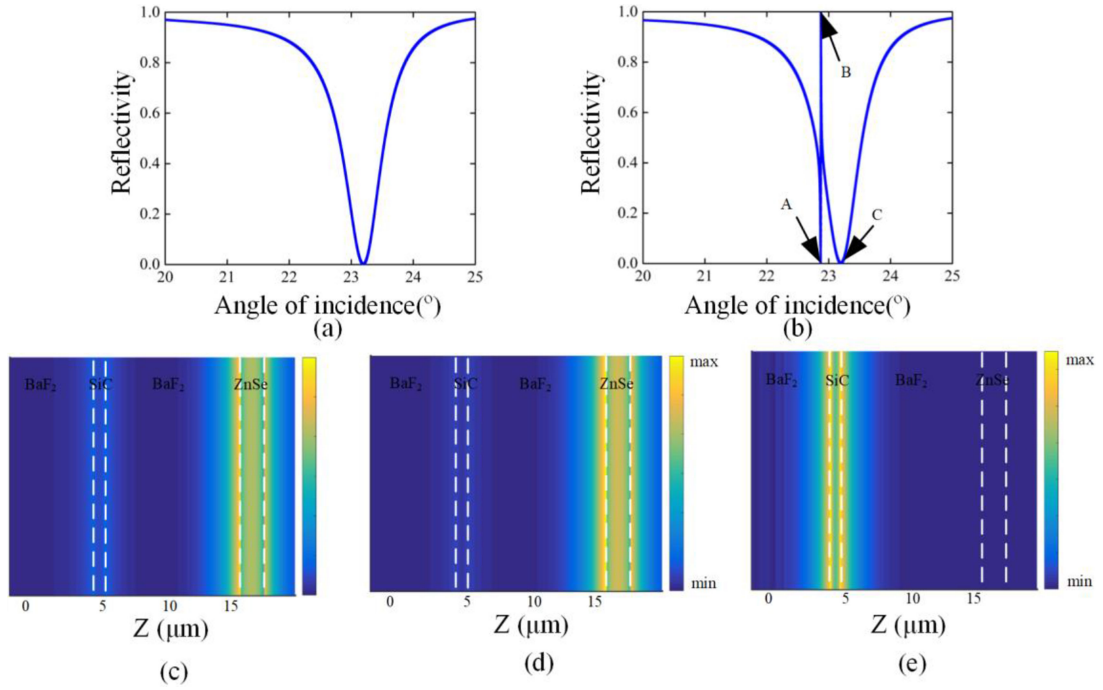

Fig. 2. (a), (b) ATR curve of the LRSPhR and the WG-LRSPhR calculated as a function of the incident angle. (c)–(e) Distributions of the electric field $|H_y|$ at the three dips as noted in Fig. 2(a). The refractive index of sensing medium is 1.332.

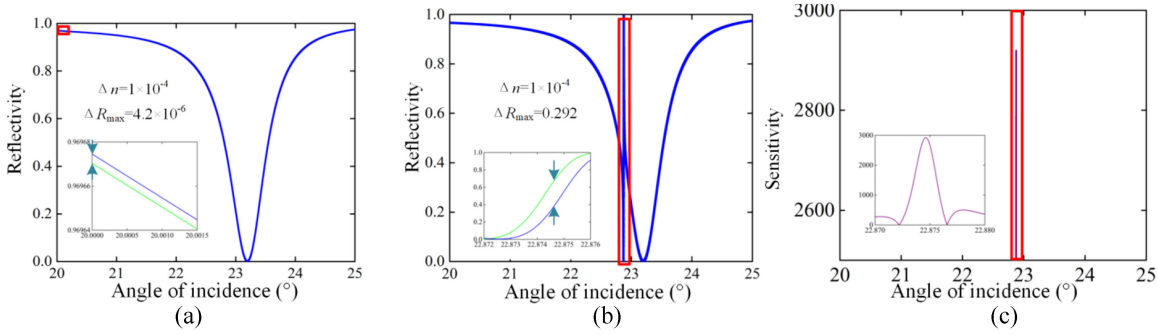

Fig. 3. (a) Variation of reflectance and sensitivity for the proposed structure with $t = 0.7$ μm, $d_2 = 12$ μm and $d_3 = 1.7$ μm, caused by an RI increase by $\Delta n = 1 \times 10^{-4}$. (b) Change in the ATR dip in conventional LRSPhR sensor with a 0.7 μm-thick SiC film deposited onto a Ge prism and a 4 μm-thick BaF_2, caused by an RI increase by $\Delta n = 1 \times 10^{-4}$. (c) Sensitivity calculated as a function of the incident angle.

Fig. 3 compares the variation of the ATR curve between the WG-LRSPhR and the conventional LRSPhR with the refractive index variation of $\Delta n = 1 \times 10^{-4}$. For the FR sensor, the structure was arranged with $d_2 = 12$ μm and $d_3 = 1.7$ μm. The change of the resonance curve is much more drastic, Fig. 3(b) comparing to the case of LRSPhR, Fig. 3(a). The sharp transition region between resonance peak and resonance dip is preferred for intensity interrogation, and the sensitivity is defined as

$$S_l(\theta) = \lim_{\Delta n \to 0} \frac{\Delta R(\theta)}{\Delta n} = \frac{\partial R(\theta)}{\partial n} \tag{2}$$

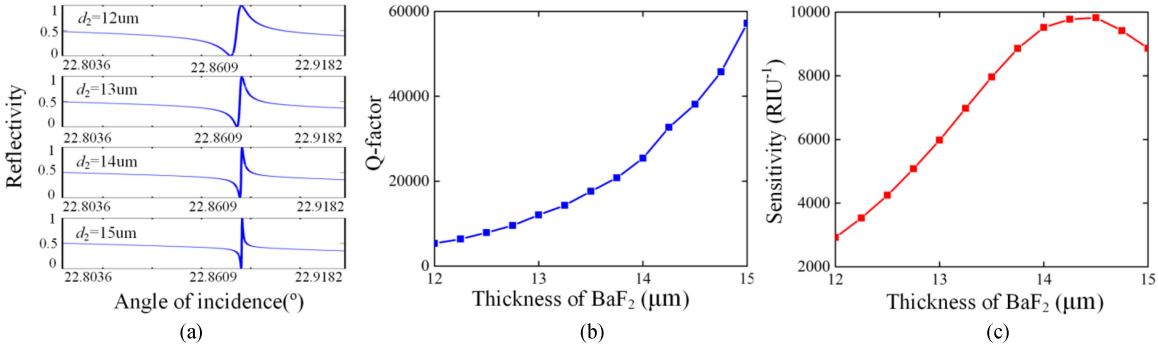

Fig. 4. (a) Resonances caused by coupling between WGM and LRSPhR with the thickness of BaF_2 increased from 12 μm to 15 μm, with d_2 fixed at 1.7 μm. (b), (c) Variation of Q-factor and sensitivity caused by the increasing of thickness of BaF_2.

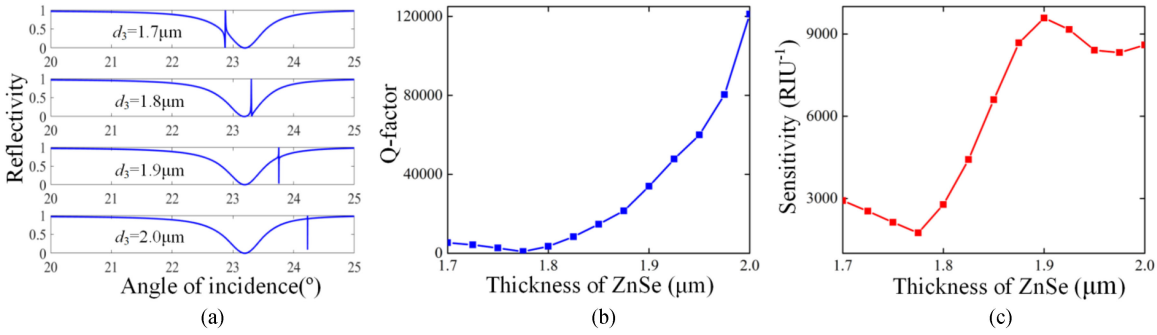

Fig. 5. (a) Resonances caused by coupling between WGM and LRSPhR with the thickness of ZnSe increased from 1.7 μm to 2.0 μm, with d_2 fixed at 12 μm. (b), (c) Variation of Q-factor and sensitivity caused by the increasing of thickness of ZnSe.

where ΔR is the reflectivity change caused by the index change Δn. The sensitivity at different angle is shown in Fig. 3(c), where the peak is defined as S_{max}. Quantitively, the S_{max} for FR is 2.92 $\times$ 10^3 RIU^{-1}, which is five orders magnitude that of the LRSPhR.

Fig. 4(a) shows ATR curves for the proposed structure with thickness of BaF_2 ranging from 12 μm to 15 μm with d_3 fixed at 1.7 μm. With thinner BaF_2 layer, the coupling is stronger and the resonance turns to be broader obviously, resulting in lower Q-factor. When $d_2 = 15$ μm, the corresponding Q-factor can be calculated as $Q = \theta/\Delta\theta = 22.8765/0.0004 = 57191$ (θ is the resonant angle of FR and $\Delta\theta$ is defined as the difference of reflection peak and dip angle). Variations of the Q-factor and sensitivity as a function of the thickness of BaF_2 are plotted in Fig. 4(b) and (c), respectively. Q-factor keeps increasing with d_2 increment, and the sensitivity maximizes as the thickness of BaF_2 at 14 μm. It can be found out that higher Q-factor doesn't correspond to higher sensitivity. This can be attributed to that though higher Q-factor gives raise a sharper resonance, the interaction between optical field and sensing medium becomes weaker due to a thicker BaF_2 layer.

ATR curves with different ZnSe thickness under the condition of $d_2 = 12$ μm are calculated and shown in Fig. 5(a). With the increment of ZnSe thickness, the position of FR peak moves to a larger incident angle. This is because thicker ZnSe layer corresponds to higher effective index of the WGM, consequently, larger incident angles are required to match the resonant condition. Fig. 5(b) shows that Q-factor keeps increasing with ZnSe thickness d_3 increment, and Fig. 5(c) demonstrates the sensitivity of proposed sensor maximizes as the thickness of ZnSe at 1.9 μm.

In the discussions above, the loss of the dielectrics is neglected. In practice, the performances of the FR are significantly affected by the loss of ZnSe. To further study the impact of the loss, various

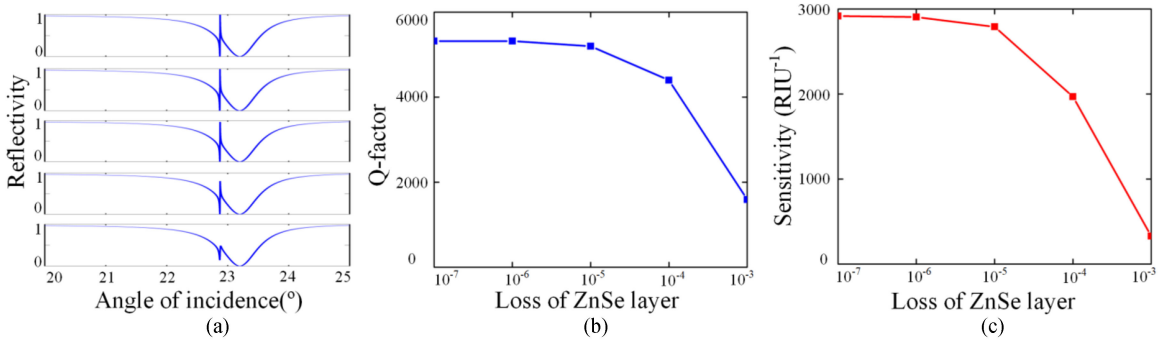

Fig. 6. (a) Variation of the loss of ZnSe on ATR curve. (b) Q-factor and (c) sensitivity in logarithmic coordinate.

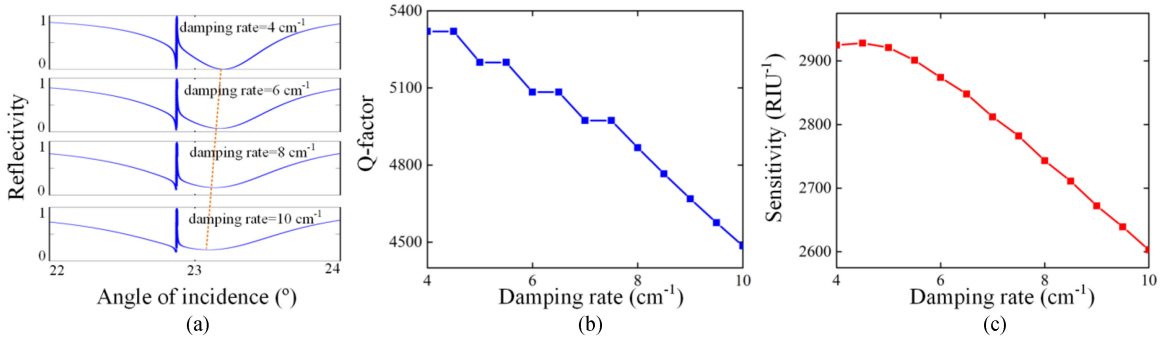

Fig. 7. (a) Impact of the damping rate on the ATR curve. (b) Q-factor and (c) sensitivity of the proposed WG-LRSPhR sensor.

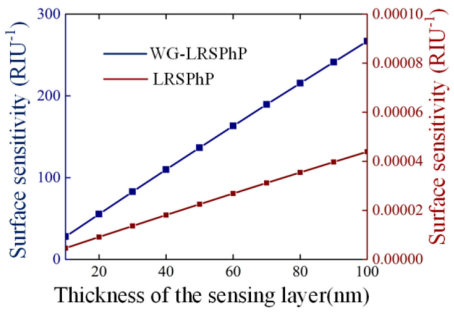

Fig. 8. Surface sensitivity with respect to proposed WG-LRSPhR sensor and the conventional LRSPhR sensor with different thickness of the dielectric (RI = 1.332) overlay.

imaginary part of ZnSe refractive index are proposed to investigate the sensing performances. With the BaF_2 layer thickness and the ZnSe layer thickness fixed to be 12 μm and 1.7 μm, the ATR curve with respect to imag(n_{ZnSe}) are shown in Fig. 6(a). FR intensity keeps decreasing, with the extinction coefficient increasing from 10^{-7} to 10^{-3}. However, when the imag(n_{ZnSe}) is smaller than 10^{-6}, the resonance changes little, which means the Q-factors are almost unchanged as verified in Fig. 6(b). Similar situation emerged with the sensitivity, as demonstrated in Fig. 6(c).

Eq. (1) is a typical dispersion relation of SiC epitaxially grown on a silicon substrate. However, if SiC is grown on other types of substrates, damping rate will be changed, leading to the change of the permittivity of SiC and consequently the sensing performance. Further study on the impact of

the damping rate are illustrated in Fig. 7. It is obvious that higher of damping rate of SiC conducts a resonance angle shift for LRSPhR, while the position of FR angle is nearly unchanged. Fig. 7(b) shows that Q-factor keeps decreasing with the increment of damping rate. For sensitivity, though it is also degraded by the damping rate, it is not as drastic as the impact of the ZnSe loss. The sensitivity can be maintained above 2600 RIU^{-1} within the investigated damping rate range, which means such structure offers a robust sensing performance on SiC damping rate.

4. Discussion and Conclusion

Other than bulk sensitivity, the surface sensitivity ($S_{surface}$) is more realistic to characterize the sensing performance in case that the sensing target possesses small size and the light-matter interaction only occurs near the interface such as DNA. Here we consider the surface sensitivity caused by a small change in the RI near the sensor's surface with nanometer scale. Fig. 8 demonstrates that the surface sensitivity of WG-LRSPhR sensor changes from 27.85 RIU^{-1} to 267.1 RIU^{-1} with the thickness of accumulate layer increases from 10 to 100 nm. Obviously, the surface sensitivity shows strong dependence on the thickness of the accumulate layer. Under the same condition, the surface sensitivity of conventional LRSPhR only changes from 4.59×10^{-6} RIU^{-1} to 4.39×10^{-5} RIU^{-1}. Results show that the surface sensitivity can be significantly improved by utilizing the FR.

Another advantage of using LRSPhR to form FR lies in the multi-parameters sensing application. For example, in biochemical sensing, the index change is always accompanied with the temperature variation, which can bring crosstalk to the sensors when only a SPR or SPhPR curve is employed. However, in the proposed sensor, though the index change induces little influence on the LRSPhR curve, the temperature change can modify it. Therefore, such configuration has the potential for simultaneously probing dual parameters. Particularly, since the LRSPhR possesses much narrower FWHM (0.9021 deg) comparing to the traditional SPhR (1.2998 deg), the sensing accuracy can be significantly improved.

In conclusion, LRSPhR is numerically demonstrated for the first time in a planer multilayer structure. The coupling between LRSPhR and WGM forms asymmetric FR which is investigated as the platform for index sensing. It demonstrates that the bulk and surface sensitivity of proposed structure can reach ~9000 RIU^{-1}, and 266.9 RIU^{-1}, respectively, which shows great enhancement comparing with the one in single resonance configuration. The resonance shape can be tailored and optimized by engineering the geometry and material loss as well. With such an excellent performance, the configuration can be a promising platform for biochemical sensing in the MIR.

References

[1] S. Gupta, A. Paliwal, V. Gupta, and M. Tomar, "Waveguide coupled surface plasmon resonance based electro optic modulation in SBN thin films," *Appl. Surf. Sci.*, vol. 458, pp. 139–144, 2018.
[2] S. Shen, A. Narayanaswamy, and G. Chen, "Surface phonon polaritons mediated energy transfer between nanoscale gaps," *Nano. Lett.*, vol. 9, no. 8, pp. 2909–2913, 2009.
[3] A. Huber, N. Ocelic, D. Kazantsev, and R. Hillenbrand, "Near-field imaging of mid-infrared surface phonon polariton propagation," *Appl. Phys. Lett.*, vol. 87, no. 8, 2005, Art. no. 081103.
[4] A. K. Sharma and A. Dominic, "Influence of chemical potential on graphene-based SPR sensor's performance," *IEEE Photon. Technol. Lett.*, vol. 30, no. 1, pp. 95–98, Jan. 2018.
[5] L. Li, T. Huang, X. Zhao, X. Wu, and Z. Cheng, "Highly sensitive SPR sensor based on hybrid coupling between plasmon and photonic mode," *IEEE Photon. Technol. Lett.*, vol. 30, no. 15, pp. 1364–1367, Aug. 2018.
[6] M. He, M. E. Bianchi, T. R. Coleman, J. T. Kevin, and A. A. Yousef, "Exploring the biological functional mechanism of the HMGB1/TLR4/MD-2 complex by surface plasmon resonance," *Mol. Med.*, vol. 24, no. 1, 2018, Art. no. 21.
[7] D. R. Shankaran, K. V. Gobi, and N. Miura, "Recent advancements in surface plasmon resonance immunosensors for detection of small molecules of biomedical, food and environmental interest," *Sens. Actuators B, Chem.*, vol. 121, no. 1, pp. 158–177, 2007.
[8] A. A. Bergwerff and F. V. Knapen, "Surface plasmon resonance biosensors for detection of pathogenicmicroorganisms: Strategies to secure food and environmental safety," *J. AOAC Int.*, vol. 89, no. 3, pp. 826–831, 2006.
[9] C. D. Geddes, *Reviews in Plasmonics 2010*. New York, NY, USA: Springer, 2011.
[10] G. Zheng, H. Zhang, L. Bu, H. Gao, L. Xu, and Y. Liu, "Tunable Fano resonances in mid-infrared waveguide-coupled Otto configuration," *Plasmonics*, vol. 13, no. 1, pp. 215–220, 2017.

[11] Y. Chen *et al.*, "Spectral tuning of localized surface phonon polariton resonators for low-loss mid-IR applications," *ACS Photon.*, vol. 1, no. 8, pp. 718–724, 2014.
[12] A. D. Dunkelberger *et al.*, "Active tuning of surface phonon polariton resonances via carrier photoinjection," *Nat. Photon.*, vol. 12, no. 1, pp. 50–56, 2018.
[13] J. D. Caldwell *et al.*, "Low-loss, infrared and terahertz nanophotonics using surface phonon polaritons," *Nanophotonics*, vol. 4, no. 1, pp. 44–68, 2015.
[14] G. Zheng, L. Xu, X. Zou, and Y. Liu, "Excitation of surface phonon polariton modes in gold gratings with silicon carbide substrate and their potential sensing applications," *Appl. Surf. Sci.*, vol. 396, pp. 711–716, 2017.
[15] X. Tan and X. Zhu, "Enhancing photonic spin Hall effect via long-range surface plasmon resonance," *opt. Lett.*, vol. 41, no. 11, pp. 2478–2481, 2016.
[16] Y. X. Jiang, B. H. Liu, X. S. Zhu, X. L. Tang, and Y. W. Shi, "Long-range surface plasmon resonance sensor based on dielectric/silver coated hollow fiber with enhanced figure of merit," *Opt. Lett.*, vol. 40, no. 5, pp. 744–747, 2015.
[17] J. Zhu, J. Li, L. Yuan, and J. Zhao, "Optimization of three-layered Au–Ag bimetallic nanoshells for triple-bands surface plasmon resonance," *J. Phys. Chem. C*, vol. 116, no. 21, pp. 11734–11740, 2012.
[18] V. S. K. Chakravadhanula *et al.*, "Equal intensity double plasmon resonance of bimetallic quasi-nanocomposites based on sandwich geometry," *Nanotechnology*, vol. 19, no. 22, 2008, Art. no. 225302.
[19] X. Zhao *et al.*, "Sensitivity enhancement in surface plasmon resonance biochemical sensor based on transition metal dichalcogenides/graphene heterostructure," *Sensors*, vol. 18, no. 7, 2018, Art. no. 2056.
[20] J. B. Maurya, A. François, and Y. K. Prajapati, "Two-dimensional layered nanomaterial-based one-dimensional photonic crystal refractive index sensor," *Sensors*, vol. 18, no. 3, 2018, Art. no. 857.
[21] A. D. Khan, M. Amin, M. Y. Iqbal, A. Ali, R. Khan, and S. D. Khan, "Twin dipole Fano resonances in symmetric three-layered plasmonic nanocylinder," *Plasmonics*, vol. 10, no. 4, pp. 963–970, 2015.
[22] G. Zheng, Y. Chen, L. Bu, L. Xu, and W. Su, "Waveguide-coupled surface phonon resonance sensors with super-resolution in the mid-infrared region," *Opt. Lett.*, vol. 41, no. 7, pp. 1582–1585, 2016.
[23] N. Muhammad and A. D. Khan, "Tunable Fano resonances and electromagnetically induced transparency in all-dielectric holey block," *Plasmonics*, vol. 10, no. 6, pp. 1687–1693, 2015.
[24] Y. Chang and Y. Jiang, "Highly sensitive plasmonic sensor based on Fano resonance from silver nanoparticle heterodimer array on a thin silver film," *Plasmonics*, vol. 9, no. 3, pp. 499–505, 2014.
[25] T. Huang, S. Zeng, X. Zhao, Z. Cheng, and P. Shum, "Fano resonance enhanced surface plasmon resonance sensors operating in near-infrared," *Photonics*, vol. 5, no. 3, 2018, Art. no. 23.
[26] S. Hayashi, D. V. Nesterenko, and Z. Sekkat, "Fano resonance and plasmon-induced transparency in waveguide-coupled surface plasmon resonance sensors," *Appl. Phys. Express*, vol. 8, no. 2, 2015, Art. no. 022201.
[27] D. V. Nesterenko, S. Hayashi, and Z. Sekkat, "Extremely narrow resonances, giant sensitivity and field enhancement in low-loss waveguide sensors," *J. Opt.*, vol. 18, no. 6, 2016, Art. no. 065004.
[28] S. Hayashi, D. V. Nesterenko, A. Rahmouni, and Z. Sekkat, "Observation of Fano line shapes arising from coupling between surface plasmon polariton and waveguide modes," *Appl. Phys. Lett.*, vol. 108, no. 5, 2016, Art. no. 051101.
[29] L. Wu, J. Guo, H. Xu, X. Dai, and Y. Xiang, "Ultrasensitive biosensors based on long-range surface plasmon polariton and dielectric waveguide modes," *Photon. Res.*, vol. 4, no. 6, pp. 53–57, 2016.
[30] Z. Sekkat *et al.*, "Plasmonic coupled modes in metal-dielectric multilayer structures: Fano resonance and giant field enhancement," *Opt. Express*, vol. 24, no. 18, pp. 20080–20088, 2016.
[31] X. Zou, G. Zheng, Y. Chen, F. Xian, and L. Xu, "Tunable and angle-independent thermal emitter based on surface phonon polariton mode in the mid-infrared range," *Opt. Mater.*, vol. 85, pp. 91–95, 2018.
[32] B. Tatian, "Fitting refractive-index data with the Sellmeier dispersion formula," *App. Opt.*, vol. 23, no. 24, pp. 4477–4485, 1984.
[33] S. Zeng *et al.*, "Graphene–MoS2 hybrid nanostructures enhanced surface plasmon resonance biosensors," *Sens. Actuator B, Chem.*, vol. 207, pp. 801–810, 2015.